A LEAD/GRAPHITE ACCUMULATOR USING AQUEOUS HYDROFLUORIC ACID

FRITZ BECK and HOLGER KROHN

*University Duisburg (GH), FB6, Fachgebiet Elektrochemie, D 4100 Duisburg 1 (F.R.G.)**

(Received May 6, 1983)

Summary

In this paper a new aqueous accumulator is described and its main advantages and disadvantages are discussed. It consists of a lead negative electrode (enveloped in a microporous separator), a 3 mm thick polypropylene loaded with natural graphite flakes (20/80) (CPP) positive electrode, and an aqueous hydrofluoric acid (40 - 60 wt.% HF) electrolyte. Both electrodes undergo very effective formation during the first five cycles and thereafter are extremely reversible. The lead works as an electrode of the second kind and the graphite as a host lattice for the intercalation of HF_2^- anions.

More than 1000 cycles were completed in 40% HF while in 60% HF 3000 cycles were exceeded. The conversion of the electrolyte and the graphite was 1% and 30%, respectively, but in special cells, up to 60% and 100% ($C_{48}F$) respective conversion was achieved. Repeated partial discharge was possible and self discharge was about 3% per day.

The cell promises to be cheap with a very good cycle life and, although the theoretical energy density is only 62 W h kg^{-1}, 30 W h kg^{-1} should be realised in practice if thin layer techniques are used.

Zusammenfassung

Es wird ein neuer wässriger Akkumulator vorgeschlagen auf der Basis von glattem Blei, umgeben von einem mikroporösen Separator, als negativer Elektrode und einer 3 mm dicken Verbundelektrode "CPP" aus 80 Gew % Naturgraphitflocken und 20 Gew % Polypropylen als Positive. Als Elektrolyt wird wässrige Flusssäure eingesetzt, vorzugsweise im Konzentrationsbereich von 40 - 60 Gew % HF. Standardbedingungen beim Zyklisieren waren Stromdichten von 3 mA cm^{-2} und Ladezeiten von 1 - 3 Stunden. Während der ersten fünf Zyklen werden beide Elektroden sehr effektiv formiert.

Blei bildet eine Elektrode zweiter Art. Der Naturgraphit dient als Wirtsgitter für die Intercalation von HF_2^- Anionen. Beide Elektroden verhalten sich ungewöhnlich reversibel, so dass mehr als 1000 Zyklen in 40% HF und mehr als 3000 Zyklen in 60% HF erreicht werden können.

*Mailing address: Lotharstrasse 63.

0378-7753/84/$3.00

Unter Standardbedingungen wurden 1% des Elektrolyten und 30% des Graphits umgesetzt. In speziellen Zellen konnten jedoch bis zu 60% des Elektrolyten und 100% des Graphits ($C_{48}F$) genutzt werden. Wiederholte Teilentladungen sind möglich. Die Selbstentladung beträgt etwa 3% pro Tag.

Die wichtigsten Vor- und Nachteile der neuen Sekundärbatterie werden diskutiert. Das zyklische Verhalten ist hervorragend. Alle Materialien sind preiswert. Die theoretische Energiedichte ist 62 W h kg^{-1}. Bei konsequenter Anwendung der Dünnschichttechnik sollten in der Praxis Werte von 30 W h kg^{-1} erreichbar sein.

---

1. Introduction

The lead–acid secondary battery is still a major means of storing electrochemical energy [1]. The main efforts to overcome some of its limitations have been directed towards improving its design and construction rather than changing the electrochemical system itself [2]. One of the few exceptions has been the use of the lead tetrafluoroborate battery to improve the degree of active mass utilization [2, 3]. In this paper we report here another approach. Keeping the negative lead electrode, the positive electrode, PbO_2, is replaced by a graphite salt electrode and aqueous hydrofluoric acid replaces aqueous sulfuric acid as the electrolyte. In such a cell both electrodes are readily formed. Composite electrodes with natural graphite have been shown to allow the reversible electrochemical intercalation of anions such as HSO_4^-, BF_4^- or ClO_4^- [4, 5] as well as HF_2^- [6] in aqueous solutions. These electrodes work as positives in the cell. The overall reaction in the case of H_2F_2 can be written as

$$C_x + 3xyH_2F_2 \underset{\text{disch.}}{\overset{\text{ch.}}{\rightleftharpoons}} [C^{y+}y(HF_2^- \cdot 2H_2F_2)]_x + xyH^+ + xye^- \quad (1)$$

where y is the 'degree of intercalation' and $1/y$ corresponds to the classical stoichiometry of graphite intercalation compounds [7]. Stages 1, 2, 3.. correspond to $1/y = 24, 48, 72..$ or $y = 0.042, 0.021, 0.014$.

The graphite salt contains "solvate acid" [8] and contrary to former findings [8, 9], high efficiencies for the intercalation process have been obtained in non-concentrated aqueous acids. It is only in these electrolytes, that metal negative electrodes are reversible. Using lead in H_2F_2, the benefits of an electrode of the second kind in secondary batteries can be verified:

$$Pb + H_2F_2 \underset{\text{ch.}}{\overset{\text{disch.}}{\rightleftharpoons}} PbF_2 + 2H^+ + 2e^- \quad (2)$$

A combination of the two electrode processes yields the cell reaction for a lead/graphite accumulator in aqueous H_2F_2:

$$Pb + 2[C_{1/y}(HF_2^- \cdot 2H_2F_2)] \underset{\text{ch.}}{\overset{\text{disch.}}{\rightleftharpoons}} PbF_2 + \frac{2}{y}C + 5H_2F_2 \quad (3)$$

The electrolyte only appears in the overall cell reaction due to conversion of solvate acid. As will be shown, HF allows a greatly simplified formation process of both electrodes compared with that in H_2SO_4 electrolyte. Some preliminary results have been published elsewhere [10 - 12].

2. Experimental

2.1. The Cell Components

2.1.1. The electrolytes used in this work were mainly 40 wt.% (22.6M) H_2F_2 (Merck, reinst) and 60 wt.% (36M) H_2F_2, made from 70 - 75% HF (Fluka, pract.). In some cases, however, mixtures of 72 wt.% (12M) H_2SO_4 (from Merck, p.a.), with 40 wt.% H_2F_2 were used for comparison.

2.1.2. The negative electrodes were smooth, 1 mm thick, sheets of 99.99% lead* which were used without further preparation. They were enveloped in most cases by a microporous separator "Daramic®" made from a polyolefin**.

As this material contains SiO_2 as a filler, which is leached out in HF solution, shrinkage had to be allowed for.

2.1.3. The positive electrodes were plates about 3 mm thick, made from 80 wt.% natural graphite flakes (Grossflocke, Kropfmühl, Bavaria) and 20 wt.% polypropylene (low crystallinity, BASF) hot pressed at 190 °C. This material (CPP) was originally developed as base electrodes for the lead dissolved secondary battery [3, 13] and for electroorganic synthesis cells [14]. The nonporous plates, in which the flakes tend to be oriented parallel to the plate surface, have an average electronic conductivity of about 0.2 - 0.5 S/cm perpendicular to the surface and 1 - 3 S/cm parallel to it. The natural graphite contains about 6% mineral components ("ash" = Al_2O_3 + SiO_2 + Fe_2O_2, etc.), which is leached out under our cycling conditions (see Section 3.3). The use of 99.9% natural graphite, which is much more expensive, was not found to improve the CPP. The surface of the plates was slightly abraded by carborundum paper to remove a polypropylene rich film before use.

2.2. Cell types

The various types of cell used in this work are shown schematically, but to scale, Fig. 1(a) - (d). All were monopolar, with the CPP electrodes polarized from both sides and the lead electrodes from one side. The current was conducted from one edge.

---

*We greatly appreciate the provision of this material by Vereinigte Zinkwerke, Stolberg.

**We are grateful to Grace GmbH, Norderstedt, (Dr W. Böhnstedt) for providing the separator.

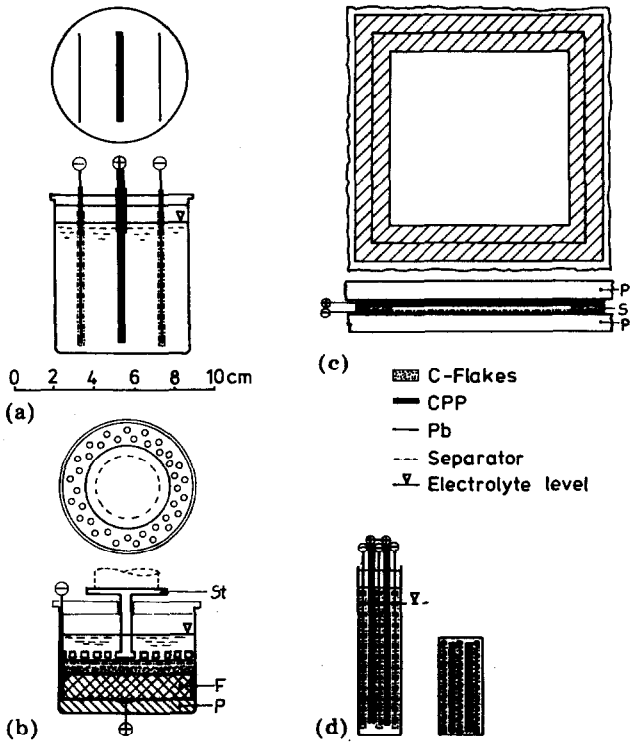

Fig. 1. Schematic representation of the cell types (drawn to scale). (a) Cylindrical cell "RC". CPP-electrode, (5 X 5 cm, total surface area = 50 cm^2). (b) Bed cell "BC". Geometrical surface area of graphite bed A = 40 cm^2. F = Feeder, P = Paraffin, St = Stamp (PVC). (c) Thin layer cell "TLC". One CPP electrode, A = 100 cm^2. P = "Pertinax"-plate, S = spacer. (d) Box cell "KC". Two CPP electrodes, A = 130 cm^2. A is the geometrical area of active CPP material.

2.2.1. The Round Cell "RC" (Fig. 1(a)) case was made from polythene (a cut bottle) with a PVC cover into which slots were machined to hold the electrodes. The upper parts of the electrodes, to about 1 cm below the level of the electrolyte, were covered with an adhesive plastic (PVC) sheet and the contacts were made at the top edge by soldering the lead plates and using two screws for the CPP electrode. The active surface of each electrode was 50 cm^2.

2.2.2. The Bed Cell "BC" (Fig. 1(b)) was also cylindrical but had a paraffin wax sealed lead through to a plate of Acheson graphite (Diabon N, Sigri) as a contact at the bottom of the cell. This was covered by a bed of natural graphite flakes (Grossflocke), normally 1.5 mm thick, a separator, and a perforated lead sheet. The horizontal stack was topped by a perforated PVC plate, and the whole assembly was compressed with a 1 kg load.

2.2.3. The Thin Layer Cell "TLC" (Fig. 1(c)) did not have a normal case but was made of a set of plates: brass / CPP / separator / lead / brass.

A natural caoutchouc elastomer gasket between the electrodes sealed in the electrolyte, which had to be injected into the cavity. The separator was a layer of paper or Darak 2000® *.

2.2.4. The Box Cell "KC" (Fig. 1(d)) contained two positive electrodes between three negative electrodes in a PVC box. The separators around the negatives were the same as those in the round cell. The total active electrode area was 130 cm^2.

2.3. Procedures

All the cycling tests were performed under the following standard conditions:

Current density (charge and discharge)	-3 mA cm^{-2}
Charge time	-1 h
End of discharge	-1.0 V
Temperature	-20 °C

Cycling was normally continued uninterrupted until the cell failed after which the electrodes were inspected and a mass balance analysis completed. The experimental conditions for the single electrode measurements are reported elsewhere [4 - 6].

3. Results and discussion

3.1. Single negative electrodes

The current/voltage characteristic of a lead electrode in 60 wt.% HF is shown in Fig. 2. The resting potential at $U_H = -240$ mV indicates that Pb/PbF_2 is an electrode of the second kind, establishing an equilibrium potential rather than a corrosion potential. Anodic polarization leads to the formation of insoluble PbF_2, which covers the electrode as a well-adhering porous film without any tendency for passivation. At negative currents the PbF_2 is reduced to slightly spongy lead. There is an initial sharp reduction peak after which the current does not fall to zero but to a steady state value between 3 and 5 mA cm^{-2}, indicating further transport limited reduction and then it increases again due to hydrogen evolution. This rise is well separated from the reduction peak due to the high hydrogen overvoltage of lead.

Upon anodic polarization, the current may rise to very high values, up to 1500 mA cm^{-2}, without any passivation. The only effect is an increase in ohmic voltage drop in the thick salt layer. Similar curves have been obtained in 40 wt.% HF, with $j_+ = 800$ mA cm^{-2} at $U_s = 0$ V and a cathodic limiting current of 1.5 mA cm^{-2} [10]. These results show that only minor overvoltages may arise in both directions if the electrode is cycled at small current densities. In contrast to this beneficial behaviour, lead passivates

*Please see second footnote on page 11.

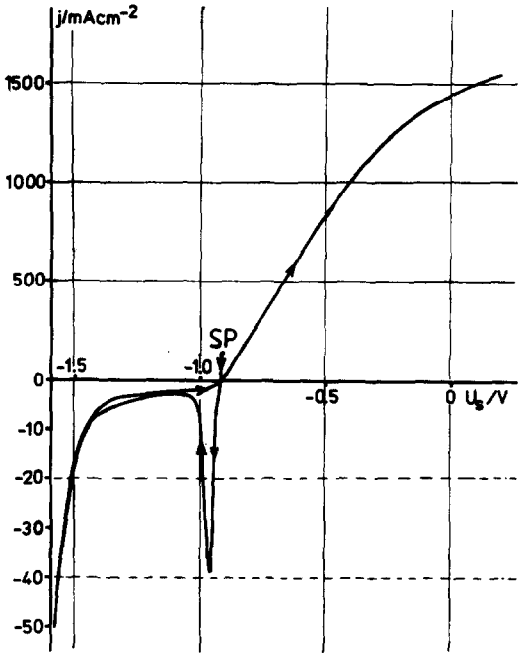

Fig. 2. Cyclic current/voltage characteristic of a lead electrode in 60 wt.% HF, saturated with PbF_2. Temperature, 30 °C, voltage scan rate 2 mV s^{-1}. SP = starting point. U_s = potential *vs.* $Hg/Hg_2SO_4/1M\ H_2SO_4$ reference electrode. After some anodic prepolarization, the measurement was primarily performed in the negative direction, at last in the positive region. Note the different current scales for positive and negative values.

very rapidly in aqueous sulfuric acid, and the cathodic reduction of $PbSO_4$ is severely limited by transport polarization. Moreover, passive anodes enter rapidly into a potential region where PbO_2 is generated [15 - 17]. An example of galvanostatic cycling experiments is shown in Fig. 3. The first polarization is cathodic, in which hydrogen is evolved while the first anodic polarization generates PbF_2 as an active mass to be consumed in the following cathodic part of the cycle. As some material may be lost, and as transport may become critical towards the end of this portion, the overvoltage increases during this charging process. This effect, however, levels out even after a few cycles. Once again, the uniqueness of Pb/PbF_2 compared with the $Pb/PbSO_4$ system which, when the current is reversed, shows only the switch between the H_2- and the O_2-electrode with the $Pb/PbSO_4/PbO_2$-processes submerged in the steep portions of potential change, is clearly demonstrated. Actually, the Planté-formation of smooth lead is much more time consuming as has been shown by galvanostatic experiments [18, 19].

The solubility of PbF_2 and $PbSO_4$ in water and in various electrolytes is compiled in Table 1.

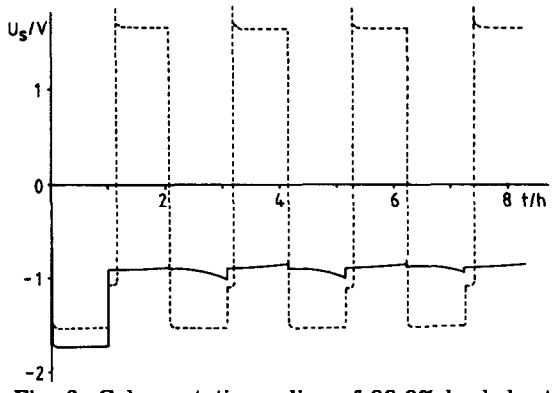

Fig. 3. Galvanostatic cycling of 99.9% lead sheet. ——, in 40 wt.% HF, saturated with PbF_2. - - - -, in 12M H_2SO_4. Temperature, 20 °C. After one hour (initially negative) polarization and a rest period of 5 min, the current is reversed for one hour. Current densities: ——, 3 mA/cm^2; - - - -, 0.5 mA/cm^2.

TABLE 1

Solubility of PbF_2 and $PbSO_4$ (mMol/l) at 20 °C

Solvent	PbF_2	$PbSO_4$
Water	2.7	0.16
40% HF*	1.1	
60% HF*	4.0	
6M H_2SO_4 [20, 21]		0.015
12M H_2SO_4 [20, 21]		0.025

The solubility of PbF_2 in water exceeds that of $PbSO_4$ by more than one order of magnitude. The solubility of PbF_2 in 40 - 60% HF, however, is more than two orders of magnitude greater than that of $PbSO_4$ in 6 - 12M H_2SO_4 [21]. This explains the lessened tendency for passivation and should allow higher degrees of active mass utilization (μ) for Pb/PbF_2 electrodes.

3.2. Single positive electrodes

Measurements with single CPP electrodes in various aqueous acids have been published already. The experimental techniques have been slow cyclic voltammetry [4, 6] and galvanostatic cycling [5, 22]. Our results show clearly, that the CPP-electrode is a very interesting positive electrode insofar as it exhibits reversible behaviour at high positive potentials. The intercalation potential decreases linearly with increasing electrolyte concentration, strongly deviating from the Nernst law, with HF giving the most positive potentials. As the current efficiency decreases at low acid concentrations, medium acid concentrations are the optimum ones for use in the battery. Moreover, these concentrations are the best compromise for the negative electrode as well. Transport of anions in the bulk of the

*Determination of PbF_2 solubility in HF by Chemische Werke Hüls is gratefully acknowledged.

intercalation electrode is slower than in the aqueous electrolyte and diffusion coefficients of about 10^{-7} cm^2 s^{-1} have been measured [4, 5, 23, 24]. This reduces the initial current densities to between 2 and 3 mA/cm^2 but a formation process at the CPP electrode, in the course of a few cycles, allows a substantial rise of current density thereafter. At constant current density, the potential is reduced by about 300 mV [5].

3.3. Cycling of cylindrical cells

Most of the cycling experiments were made using cylindrical cells of the simple design shown in Fig. 1(a). Some typical results are given in Table 2. The conversion of electrolyte (β_E) under standard conditions (1 h charge at 3 mA cm^{-2}) was as low as about 1%. The conversion of graphite (β_G) in CPP, however, was appreciably higher. These figures refer to a limit of $C_{48}F$ (second stage), as the first stage $C_{24}F$ [7, 25] does not seem to be stable in aqueous acids [26]. The initial cycles differed appreciably from the cycles in the steady state as Fig. 4 shows. The first charging voltage exceeded 3 V due to hydrogen evolution at the negative electrode (lead). The positive electrode determined the first discharge, thus providing only a limited amount of PbF_2, which was reduced during the equivalent potential step of the second charge. The capacity of the positive electrode, however, increased rapidly as it was formed [5], and this is reflected by an enhanced voltage step in the charging curve. In the steady state, only 5 - 10% at the end of the charge curve was at higher voltages, *cf.* Fig. 8 in ref. 9.

This interpretation was confirmed by an experiment in which a two hour charge with inversed polarity preceded the standard cycling. In this case PbF_2 accumulated on the surface of the negative lead electrode, and was used in the following cycles. Even under these conditions, while the positive is undergoing a primary formation process, the charge voltage is higher than in the steady state [5].

The general behaviour during long term cycling in 60% HF, which is superior to 40% HF, is shown in Figs. 5 and 6. The voltages are only slightly

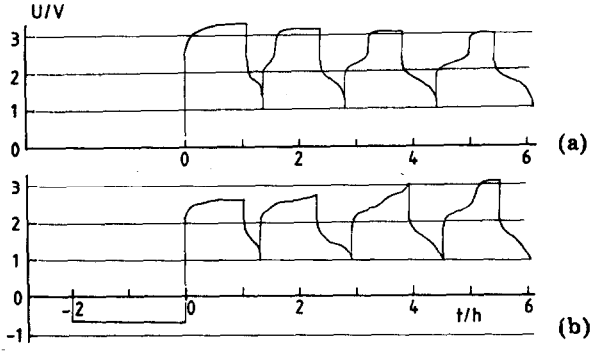

Fig. 4. Initial cycles of a Pb/CPP "RC" cell in 40% HF. One hour charge, 3 mA/cm^2, discharge to 1.0 V, (a) start with lead as a negative, (b) start with lead as a positive (two hour prepolarization at inverted polarity).

TABLE 2

Experimental cycling results with the cylindrical cell "RC" at room temperature
Lead electrodes with Daramic® separator. Discharge with the same current density as the charge until an end voltage of 1.0 V.
β_G = 100% at $C_{48}F$.

No.	Run	Electrolyte	CPP positive			Charging		$\bar{U}_{ch}$ (V)	$\bar{U}_{disch}$ (V)	α (%)	β_E (%)	β_G (%)	Z
			A/cm²	d/cm	mC/g	j_{ch} (mA cm^{-2})	t_{ch} (h)						
1	ZZ24	40% HF	50	0.3	10	3	1	2.20	1.75	97	0.6	32	863
2	ZZ53	40% HF	50	0.3	10	3	2	2.2	1.8	96	1.2	64	147
3	ZZ65	40% HF	50	0.14	4.6	3	1	2.3	1.4	90	0.6	70	47
4	ZZ58	60% HF	50	0.3	10	3	1	2.1	1.7	99	0.4	32	3250
5	ZZ95	60% HF	50	0.3	10	3	2	2.1	1.7	98	0.8	64	265
6	ZZ67	60% HF	50	0.3	10	3	3	2.07	1.7	95	1.2	96	78
7	ZZ78	60% HF	50	0.3	10	5	1	2.15	1.68	98	0.65	53	> 70
8	ZZ71	60% HF	50	0.3	10	5	2	2.2	1.65	95	1.3	106	22
9	ZZ77	60% HF	50	0.3	10	6.5	2	2.3	1.6	70	1.7	140	5
10	ZZ11	30 V 40% HF 70 V 12M H_2SO_4	50	0.3	10	3	1	2.2/2.9	1.3	75	2.24 (H_2SO_4 inert)	32	87

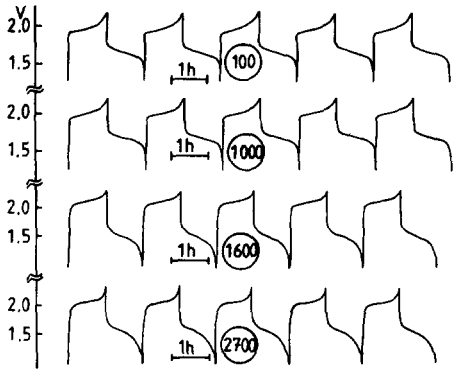

Fig. 5. Long term cycling of Pb/CPP "RC" cell in 60% HF. $j_{ch} = j_{disch} = 3$ mA/cm^2. One hour charge, discharge to 1.0 V. The circled figures are the elapsed cycles, *cf.* run No. 4 of Table 2.

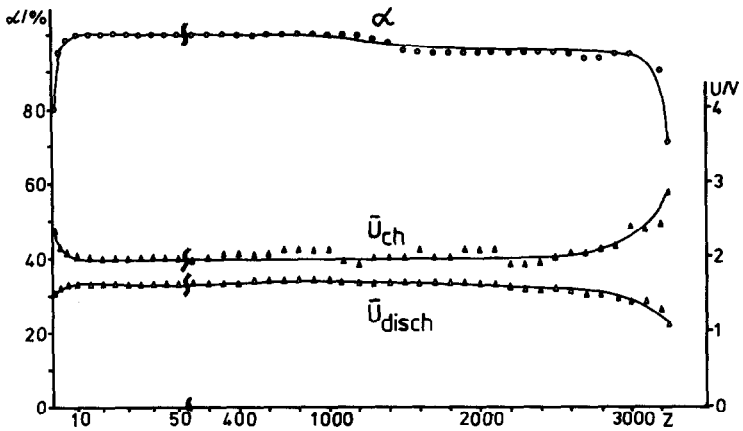

Fig. 6. Current efficiency (α), average charge voltage ($\bar{U}_{ch}$) and discharge voltage ($\bar{U}_{disch}$) as a function of cycle number. The same cell and the same conditions as in Fig. 5.

less (see Table 2) and the second voltage step in the charging curve almost disappeared, reflecting the improved current efficiency at the positive electrode. Current efficiency reached steady state after about five cycles and remained constant throughout the whole cycle life. Similarly, there were no significant changes in the average charge ($\bar{U}_{ch}$) and discharge ($\bar{U}_{disch}$) voltages until the end of cycle life. This general behaviour was observed during the other runs, and Fig. 5 shows a series of charge/discharge characteristics at differing stages of the cell's life. Breakdown of the cell was preceded by a degeneration of the discharge curves, which can also be seen in Fig. 5.

An important factor in obtaining a long cycle life was the microporous separator (Daramic®) around the lead electrode. Without this a lead sponge

grew rapidly and irregularly from the surface into the bulk of the electrolyte.

At the end of cycle life, the electrodes were inspected. Normally, a thin, gray layer was found to have accumulated between the surface of the lead electrode and the separator although the bulk of the lead was virtually unchanged, thus showing that material losses were compensated by an accumulation of corrosion products. Even oxygen enhanced corrosion at the electrolyte surface, which we have observed in the case of stirred 12M H_2SO_4 on cycling experiments with *Cu*/CPP-cells, was never significant in nonstirred aqueous HF. The CPP electrodes, on the other hand, were found to be somewhat swollen (by 20 - 50%) after prolonged cycling. Enhanced swelling was often found at the electrolyte surface level or about 1 cm below [3], as shown in Fig. 7. The mechanical integrity, however, was never lost, even after more than 3000 cycles. Usually no dispersed graphite particles could be observed as is the case with natural graphite or highly oriented pyrolitic graphite, HOPG, which has been extensively used for about ten years for physical measurements [27] but which delaminates even after two or three cycles and cannot be recharged. Thus, the CPP electrode provides a very simple and economical solution of this problem. The chemical analysis of a CPP electrode (run ZZ58) which, after 3250 cycles, was crushed, washed with water and dried at 40 °C is given in Table 3.

The components C/H/F comprise nearly 100% of the total mass, indicating almost complete removal by leaching of ash components originally present in the natural graphite. This view is further supported by the mass loss of CPP, which is of the same order as the ash content of natural graphite. The final hydrogen content is slightly below the theoretical value and the difference corresponds exactly to the fluorine content, which may be due to a slight fluorination of polypropylene:

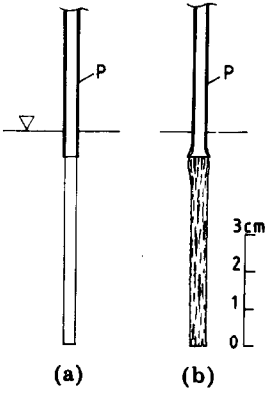

Fig. 7. Schematic representation of CPP-plate electrode. Edge view. (a) Before, (b) after extended cycling in aqueous HF. ▽, original location of electrolyte level; P = plastic coating.

TABLE 3

Chemical analysis of CPP, run ZZ58, after the last (3250th) discharge (CH-determination under the addition of V_2O_5)

	Found (wt.%)	Mole ratio found	CPP, initial mole ratio	$CH_{0.38}(HF_2 \cdot 2H_2F_2)_{0.021}$ calculated mole ratio
C	91.22	1.00	1.00	1.00
H	2.62	0.34	0.38	0.49
F	5.56	0.038	—	0.126
	99.40			

$$-CH_2- + F^- \longrightarrow -CHF- + H^+ + 2e^- \quad (4)$$

The fluorine may, however, also be covalently bound in the graphite. It does not seem to be a salt like compound, for this would lead to an enhanced hydrogen content, *cf.* last column of Table 3.

Mixtures of 12M H_2SO_4 and 40% HF have been used as electrolyte. A typical result of cycling under standard conditions is shown in Fig. 8. The voltage behaviour and α were inferior to the results in the absence of H_2SO_4. Moreover, the reduction of lead salt was not completed during each charge cycle, as indicated by the long voltage step at higher potentials. At the end of life the lead electrode had disintegrated into greyish corrosion product lamellae.

Experiments 2, and 5 - 9 in Table 2 were undertaken to increase the conversion (β_G) of the graphite by increasing the current density and/or charge time. As the transport time of intercalated anions in CPP is given by:

$$\tau_1 = \frac{L^2}{2D} \quad (5)$$

and must be equated (where L = transport length) to the charge time:

$$t_{ch} = \frac{Q_A}{j} \quad (6)$$

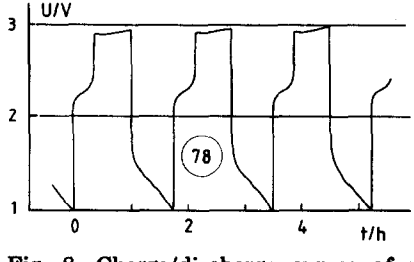

Fig. 8. Charge/discharge curves of a Pb/CPP "RC" cell. 40% HF (30 vol%) and 12M H_2SO_4 (70 vol%). $j_{ch} = j_{disch} = 3$ mA/cm^2. 1 h charge, discharge to 1.0 V. Cycles 77 - 79 of run No 10 in Table 2. Note the increasing charging voltages indicating the near end of cycle life (87 cycles).

the maximum current density is given by:

$$j = \frac{2DQ_A}{L^2} \tag{7}$$

L and Q_A are interlinked by Faraday's law. Under standard conditions (3 mA/cm^2, 1 h charge), Q_A is 1.08 A s/cm^2 and L = 0.05 cm. This, together with a diffusion coefficient of 10^{-7} cm^2 s^{-1} [4, 23, 24], gives j = 0.1 mA cm^{-2}. The possible current densities, however, are two orders of magnitude higher, as the transport length is appreciably reduced during the formation process [4, 5]. The cycling experiments in Table 2 confirm these former findings.

Finally, the upper limit seems to be a maximum concentration of $C_{48}F$, see column β_G of Table 2. Approaching this limit, or even exceeding it, leads to a dramatically reduced cycle life. As is shown by run 6 and Fig. 9, however, reversible cycling of the cell is achievable over some period with conversion almost to $C_{48}F$. Experiment 3 shows that *thin* electrodes with "edge on" contacts have additional drawbacks. One is a greater sensitivity to differences between the current drain on both sides, leading to a marked bending of the electrode.

Some runs have been made with partial charge and discharge. The standard experiment in 60% HF (1 h charge at 3 mA cm^{-2}) was, for example, reduced to 0.5 h charge and discharge after 30 cycles of formation. In this case, 520 cycles were possible before the depletion of the stock of 1 h capacity. These results will be separately discussed in further detail [22].

Several cycling experiments were interrupted periodically after charge and discharge was only started after an open circuit rest period (t_{rest}). From the deficit in discharge capacity (ΔQ_{disch}) an average corrosion current density (j_{corr}) could be calculated from:

$$j_{corr} = \frac{\Delta Q_{disch}}{t_{rest}} \tag{8}$$

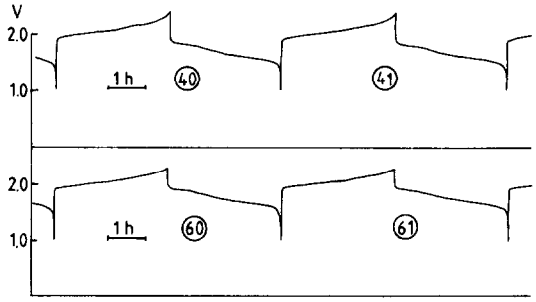

Fig. 9. Cyclic charge/discharge curves of Pb/CPP "RC" cell in 60% HF. $j_{ch} = j_{disch}$ = 3 mA/cm^2. 3 h charge, discharge to 1.0 V after 34 one hourly formation cycles of run No. 6 in Table 2.

In Table 4, some evaluations of this kind are presented for both cylindrical (RC) and for bed (BC) cells discussed below.

TABLE 4

Self discharge of the cells (cycling under standard conditions)

Cell	Electrolyte (% HF)	t_{rest} (h)	ΔQ_{disch} (A h cm^{-2})	j_{corr} (mA cm^{-2})
RC	40	65	7.5×10^{-4}	0.012
RC	60	65	3×10^{-4}	0.005
RC	60	120	4.5×10^{-4}	0.004
BC	40	83	2×10^{-3}	0.025
BC	60	60	1.2×10^{-3}	0.020

The corrosion current densities are in the range 4 - 12 μA cm^{-2}, confirming former results obtained with single electrodes [5].

3.4. Cycling of bed cells

Table 5 gives some results for experiments using cells of the type shown in Fig. 1(b) and described in Section 2, with 40 and 60% HF. Typical charge/discharge curves in 60% HF are shown in Fig. 10. By comparison with Fig. 5, the step at the end of the charging curve is more pronounced, corresponding to a lower current efficiency (93% *vs.* 99%). Moreover, the corrosion current density is higher by a factor of 4 - 5, see Table 4. This is contrary to former results with graphite bed electrodes contacted with a platinum grid, where j_{corr} was extremely low (≈ 1 μA cm^{-2}) [28] and may

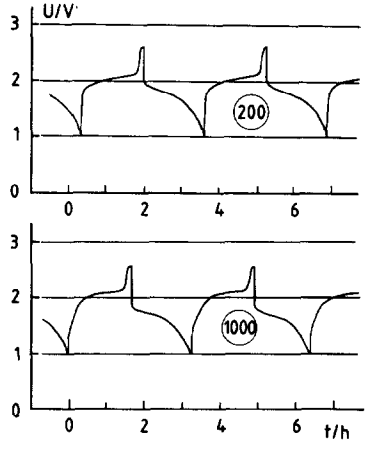

Fig. 10. Charge/discharge curves of a Pb/natural graphite "BC" cell in 60% HF. $j_{ch} = j_{disch} = 3.75$ mA cm^{-2}, 1.67 h charging. Discharge to 1.0 V. *cf.* run No. 2 in Table 5. The curves of the 200th and 1000th cycles are shown.

TABLE 5

Experimental cycling results with cells other than cylindrical cell "RC" at room temperature
Lead electrodes with Daramic® separator, in the case of TLC with paper or Darak 2000® separator. $j_{ch} = j_{disch}$. Discharge end voltage 1.0 V. $\beta_G = 100\%$ at $C_{48}F$.

No.	Run	Cell	Electrolyte (% HF)	CPP positive			Charging		$\bar{U}_{ch}$ (V)	$\bar{U}_{disch}$ (V)	α (%)	β_E (%)	β_G (%)	Z
				A/cm^2	d (cm)	m_c (g)	j_{ch} (mA cm^{-2})	t_{ch} (h)						
1	Z6b	BC	40	40	0.15	9.4	3.75	1	2.1	1.7	90	3	35	664
2	Z7	BC	60	40	0.15	9.4	3.75	1.67	2.1	1.65	93	3.1	58	>1100
3	ZZ49	KC	40	130	0.3	26	2	1	2.13	1.8	95	6.4	22	1701
4	ZZ120	KC	60	130	0.3	26	3	1	2.15	1.7	90	6.1	32	> 815
5	ZZ121	LC (large)	60	224	0.6	87	2.3	1	2.3	1.4	95	1.8	13	130
6	ZZ125	TLC	40*	50	0.07	4.6	3	1	2.2	1.5	60	30	70	105
7	Z36	TLC	40	100	0.3	40	3	1	2.15	1.75	94	59	16	> 200
8	Z37	TLC	60	100	0.3	40	3	1.67	2.1	1.8	97	62	16	> 300

*Thickened with 1% Kelzan®.

be due to attack of the carbon feeder, which was detected at the end of cycle life. The graphite flakes were virtually unchanged.

As the bed depth was only 1.5 mm, a uniform current distribution can be assumed throughout the bed. Experiments with much deeper beds are interpreted in terms of decreasing current density with increasing bed depth [29]. The voltage change during discharge is much more pronounced than in the case of CPP electrodes.

3.5. Cycling of plate cells with higher electrolyte conversion

Special plate cells, the "box cell" KC and the "thin layer cell" TLC, (see Figs. 1(d) and 1(c)), have been constructed to achieve a higher conversion of electrolyte (β_E). This was achieved by increasing the electrode surface area relative to the electrolyte volume which was kept small by limiting the interelectrode gap up to 0.5 mm. The results obtained by cycling these cells are included in Table 5. It is shown that, even with high electrolyte conversion (30 - 60%), satisfactory behaviour of the cell was achievable. Under these conditions, however, the HF concentration reaches potentially damaging levels in the middle of each cycle.

There are two ways of scaling up the box cell. Normally dense packed electrodes, both with a total surface area of 130 cm^2, were connected in parallel. In a "large box cell" two lead electrodes were used to sandwich a single CPP electrode. The latter had a total surface area of 224 cm^2. A further improvement should be possible by using bipolar electrodes, as shown in Fig. 1(d) (the "KC" cell), but a problem may arise at the interface electrode. A possible solution to this is mentioned in Section 4.3, although it has not yet been proven experimentally.

Charge/discharge characteristics of a box cell in 40% and 60% HF are shown in Fig. 11. The curves are very similar to the corresponding results

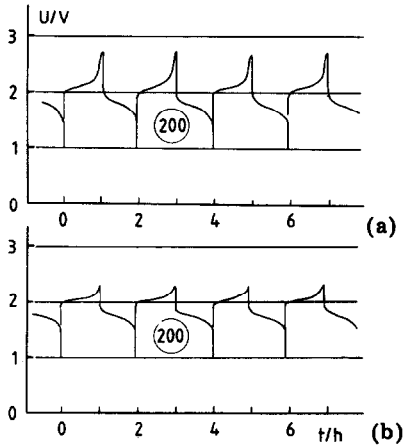

Fig. 11. Cyclic charge/discharge curves of a Pb/CPP "KC" cell. (a) 40% HF, 2 mA cm^{-2}, 1 h charge; (b) 60% HF, 3 mA cm^{-2}, 1 h charge. In both cases, the curves at the 200th cycle are shown.

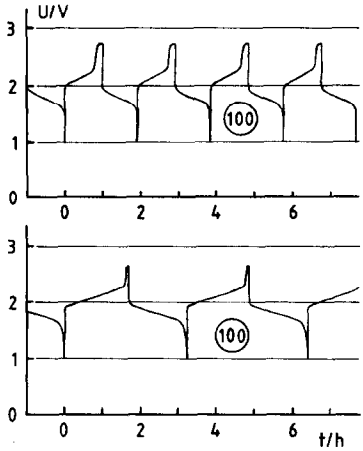

Fig. 12. Cyclic charge/discharge curves of a Pb/CPP "TLC" cell. (a) 40% HF, 3 mA cm^{-2}, 1 h charge; (b) 60% HF, 3 mA cm^{-2}, 1.67 h charge. In both cases, the curves at the 100th cycle are shown.

in the cylindrical cell and to those for the thin layer cell, as shown in Fig. 12. In the latter case, however, the step at the end of the charging period is more pronounced, indicating some loss in current efficiency due to a high electrolyte conversion (β_E).

4. Concluding remarks

4.1. Aqueous HF as an electrolyte

The main objective of this work was to demonstrate the benefits of aqueous HF, predominantly in a concentration range of 35 - 65%, as an electrolyte for the rechargeable lead/graphite cell [11]. From a practical point of view (resistivity, vapor pressure, toxicity, and current efficiency) [5], these electrolytes are superior to 100% HF.

The chemical composition of the graphite loaded polypropylene (CPP) electrode after prolonged cycling showed no evidence of irreversible graphite oxide formation in 60% HF. The fluorine found in the electrode seemed to be bound to the polypropylene rather than to the graphite (see Section 3.3.). Even if we assume a graphite fluorination, the degree of fluorination would be rather low ($CF_{0.05}$). Covalently bound fluorine in graphite was found to be a useful positive electrode in primary lithium cells with organic electrolytes [2, 30] and similar systems with a very limited rechargeability have also been described elsewhere [2, 31, 32].

In contrast to cells with HF the final composition of the CPP electrode of a Cu/CPP cell with 12M H_2SO_4 electrolyte was, after 3710 cycles, $C(HSO_4 \cdot 2H_2SO_4)_{0.0028} \cdot OH_{0.008}$ and there was light, irreversible formation of the graphite oxide according to:

$$C_x + H_2O \longrightarrow C_x{-}OH + H^+ + e^- \qquad (9)$$

4.2. Cyclic behaviour

Our results clearly show that it is the positive electrode which limits the cycle life albeit at levels exceeding 3000 cycles under standard conditions. This is primarily due to the inherent low concentration of intercalant in the graphite host lattice, the upper limit being $C_{48}F$ for 40 - 60% HF. Mechanical problems associated with exfoliation limit the cycle life in the case of natural graphite pieces, or pyrolytic graphite, to only 2 or 3 cycles and it is the composite CPP electrode which enabled such extended cycle lives to be realised. Bed electrodes were not a viable alternative so long as platinum alone is acting as an absolutely stable feeder [28]. The ultimate limitation of the CPP electrode seems to be due to irreversible alterations in the composite electrode texture rather than in solid state degeneration of the graphite flakes.

Assuming that any irreversible electrode reactions occur during the charge period with current efficiency ($\lambda_{irr,1}$) the chemical nature of this side reaction may be well represented by reaction (9). For water decomposition and/or carbon oxidation to CO_2, the current efficiency will be ($\lambda_{irr,2}$). In contrast to the first mechanism, the reaction products O_2 and CO_2 do not accumulate on or in the electrode. These two irreversible electrode reactions are to be compared with the reversible intercalation reaction (λ_{rev}). Thus

$$\lambda_{rev} + \lambda_{irr,1} + \lambda_{irr,2} = 1 \tag{10}$$

As the total (charge/discharge) current efficiency (α_+) of the electrode involves the current efficiency and the efficiency of the discharge process (ϵ_{rev}) as the second factor

$$\alpha_+ = \lambda_{rev}\epsilon_{rev} \tag{11}$$

and, as α_+ is normally found to be 98 - 99% in the steady state, the irreversible portions cannot be very high.

The irreversibly generated product in the solid state accumulates per cycle to the following extent:

$$N_{+,irr} = \lambda_{irr,1}\frac{j_{ch}t_{ch}}{zF} \tag{12}$$

where $N_{+,irr}$ is the mole number per unit area. The total capacity in the solid state can be written as (*cf.* eqn. (5) in ref. 10):

$$N_{+,max} = \frac{L\rho y w}{M_C z} \tag{13}$$

where L is the active thickness of the electrode, ρ(=1.70 g/cm^3) is the density of CPP, w(=0.80 × 0.94) the graphite concentration and $M_C = 12$, $z = 1$. From the last two equations, the maximum number of cycles (Z_{max}) is given by:

$$Z_{max} = \frac{N_{+,max}}{N_{+,irr}} = \frac{1}{\lambda_{irr,1}}\frac{FL\rho w}{j_{ch}t_{ch}M_C}\,y \tag{14}$$

Under standard conditions (L = 1 mm, j_{ch} = 3 mA/cm^2, t_{ch} = 1 h), with Z_{max} shown experimentally to be 3250, and with y = 0.05 (see Section 4.1.), $\lambda_{irr,1}$ as calculated from eqn. (14) is 1.5×10^{-3}. Thus, the irreversible change of the host lattice per cycle in terms of the current efficiency is only about 0.15%.

4.3. Theoretical and practical energy density

The *theoretical* energy density of the accumulator can be calculated from eqn. (3), with x = 1, y = 0.021, $Q = 2 \times 0.021 \times 26.8$ A h = 1.13 A h, U_o = 1.8 V*, to be $E_{s,th}$ = 61.6 W h/kg. This is a rather low figure.

Assuming, however, that the active mass utilizations (μ) are high:

Pb μ = 100%
C μ = 75% (C in CPP as $C_{48}F$)
HF μ = 25% (cycling of 65% down to 40% HF)

a practical energy density of 38 W h/kg is derived. If bipolar electrodes are used with thin separators and thin barriers of soot filled plastics between the active mass layers (see Fig. 13) a practical figure well above 30 W h/kg should be achievable.

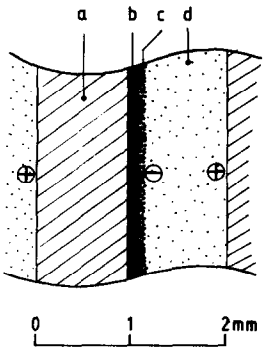

Fig. 13. Schematic representation of a bipolar cell structure with thin layer technique. (a) CPP, 1 mm; (b) plastic, filled with carbon black, 0.1 mm; (c) Pb/PbF_2, 0.05 mm; (d) electrolyte (40....65% HF) + separator, 0.7 mm.

4.4. Costing

Low costs make this accumulator very attractive. Natural graphite, polypropylene, HF, and lead are cheap and readily available and the manufacturing costs are also low. This advantage together with the high cycle life could outweigh the two inherent drawbacks, low energy density and impact on the environment, of HF and lead. At least, when the raw materials cannot be reused.

*Practical value for 40 - 60% HF rather than the lower value for 100% HF.

In recent years, new synthetic materials such as polyacetylene and poly-*p*-phenylene have become available by organic synthesis, starting from a petrochemical feedstock. As this is a very interesting aspect from a practical point of view, interest in these systems is growing. The original proposal to use these polymers in nonaqueous batteries in combination with Li [33, 34] is severely hindered by problems at the negative. Most recently, aqueous electrolytes have been shown to work satisfactorily [35, 36] and the next step will be to complete them with lead, zinc or iron as typical negative electrodes. The results obtained with such a system must be compared with the results reported here.

Acknowledgements

The authors acknowledge financial support of this work by MWF (Minister of Science and Research) of Nordrhein-Westfalen. We express our gratitude to BASF Aktiengesellschaft, Ludwighafen, especially Drs. Boehlke, Theysohn and McKee, for kindly providing CPP material. Technical assistance by H. Junge, W. Kaiser, R. Herrmann and A. Zahn is very much appreciated.

List of symbols and abbreviations

α	Current efficiency
α_+	Individual current efficiency at the positive
β_E	Conversion of electrolyte
β_G	Conversion of graphite (β_G = 100% for $C_{48}F$)
ϵ_{rev}	Current efficiency for discharge
λ_{rev}	Current efficiency for intercalation (charging reaction)
λ_{irr}	Current efficiency for irreversible side reactions during charge
μ	Active mass utilization
ρ	Density
τ_1	Transport time constant
A	Area of electrode
CPP	Composite electrode of graphite and polypropylene
D	Diffusion coefficient of intercalated anions
d	Thickness of electrode
$E_{s,th}$	Theoretical energy density
F	Faraday constant
HOPG	Highly oriented pyrolytic graphite
j	Current density
j_+	Anodic current density
j_{ch}	Current density during charge
j_{disch}	Current density during discharge
j_{corr}	Corrosion current density

L	Transport length
L	Active thickness of CPP electrode
m	Mass
M	Atomic mass
N_+	Mole number per unit area
Q	Charge
Q_A	Charge density
ΔQ_{disch}	Deficit in discharge capacity
t	Time
t_{ch}	Charge time
t_{rest}	Resting period
U	Cell voltage
U_o	Thermodynamic cell voltage
$\bar{U}_{ch}$	Average charge voltage
$\bar{U}_{disch}$	Average discharge voltage
U_H	Potential *vs.* SHE
U_s	Potential *vs.* $Hg/Hg_2SO_4/1M\ H_2SO_4$ reference electrode
w	Portion (wt.) of graphite in CPP
y	Degree of intercalation
z	Number of electrons
Z	Cycle number

References

1 M. Barak, in M. Barak (ed.), *Electrochemical Power Sources*, Peter Peregrinus Ltd., Stevenage, 1980.
2 F. Beck and K.-J. Euler, *Elektrochemische Energiespeicher*, Vol. 1, VDE-Verlag, Berlin, 1983.
3 F. Beck, Entwicklung eines Blei-Tetrafluoboratakkumulators, *BMFT Res. Rep. T 79 - 142*, 1979 (BASF AG).
4 F. Beck, H. Junge and H. Krohn, *Electrochim. Acta, 26* (1981) 799.
5 F. Beck, H. Krohn and W. Kaiser, *J. Appl. Electrochem., 12* (1982) 505.
6 F. Beck, W. Kaiser and H. Krohn, *Angew. Chem. Suppl.*, (1982) 57.
7 W. Rüdorff and U. Hofmann, *Z. Anorg. Allg. Chem., 238* (1938) 1.
8 W. Rüdorff, *Z. Anorg. Allg. Chem., 254* (1947) 319; *Angew. Chem., 60* (1948) 74.
9 W. Rüdorff, Graphite intercalation compounds, *Adv. Inorg. Chem. Radiochem., 1* (1959) 223.
10 F. Beck and H. Krohn, *DECHEMA — Monogr., 92* (1982) 57.
11 F. Beck, H. Junge, W. Kaiser and H. Krohn, *German Pat. Appl. (DOS) DE 3136 161 A1* (12.9.1981).
12 F. Beck, *Electrotechniek (Netherlands), 61* (1983) 178.
13 F. Beck, R. Wurmb and K. Boehlke, *German Pat. Appl. 2 532 512*, BASF, 1975.
14 D. Degner, in N. L. Weinberg (ed.), *Techniques of Electroorganic Synthesis*, Part III, Wiley, New York, 1982.
15 H. S. Panesar, in D. H. Collins (ed.), *Power Sources 3*, Oriel Press, Newcastle upon Tyne, 1971, p. 79.
16 Th. F. Sharpe, *J. Electrochem. Soc., 122* (1975) 845.
17 J. G. Sunderland, *J. Electroanal. Chem., 71* (1976) 341.
18 B. N. Kabanow and D. I. Leikis, *Z. Elektrochem., 62* (1958) 630.
19 E. Tarter and K. Ekler, *Can. J. Chem., 47* (1969) 2191.

20 D. N. Craig and G. W. Vinal, *J. Res. Nat. Bur. Stand., 22* (1939) 55.
21 S. E. Afifi, W. H. Edwards and N. A. Hampson, *Surf. Technol., 4* (1976) 173.
22 F. Beck and H. Krohn, to be published in *J. Electroanal. Chem.*
23 F. Beck, H. Junge and H. Krohn, in D. H. Thompson (ed.), *Power Sources 8*, Academic Press, London, 1981.
24 H. Krohn, to be published in *Ber. Bunsenges. Phys. Chem.*
25 W. Rüdorff, *Angew. Chem., 60* (1948) 74.
26 Elizabeth Rhodes, in D. H. Collins (ed.), *Power Sources 1966*, Oxford, 1967, p. 1.
27 M. S. Dresselhaus and G. Dresselhaus, *Adv. Phys., 30* (1981) 139 - 326.
28 H. Krohn, F. Beck and R. Herrmann, *Chem.-Ing.-Techn., 54* (1982) 530.
29 A. Inioui, A. Métrot and A. Storck, *Electrochim. Acta, 27* (1982) 1247.
30 *US-Pat. 3 700 502* (Matsushita Electric Ind., 1972, inventors N. Watanabe and M. Fukuda).
31 D. N. Bennion *et al., US Pat. 4 009 323*, 1977.
32 S. L. Deshpande and D. N. Bennion, *J. Electrochem. Soc., 125* (1978) 689.
33 P. J. Nigrey, D. McInnes, D. P. Nairns and A. G. MacDiarmid, *J. Electrochem. Soc., 128* (1981) 1651.
34 L. W. Shacklette, R. L. Elsenbaumer, R. R. Chance, J. M. Sowa, D. M. Ivory, G. G. Miller and R. H. Baughman, *J. Chem. Soc., Chem. Commun.*, (1982) 361.
35 A. G. MacDiarmid, M. Aldissi, R. B. Kaner, M. Maxfield, R. J. Mammone and A. J. Heeger, *Abstr. Conference Internationale sur la Physique et la Chimie des Polymerconducteurs, Les Arcs*, Dec., 1982.
36 F. Beck and A. Pruss, *Electrochim. Acta*, in press.